

Distributing Collaborative Multi-Robot Planning with Gaussian Belief Propagation

Aalok Patwardhan¹, Riku Murai² and Andrew J. Davison¹

Abstract—Precise coordinated planning enables safe and highly efficient motion when many robots must work together in tight spaces, but this would normally require centralised control of all devices which is difficult to scale. We demonstrate a new purely distributed technique based on Gaussian Belief Propagation on multi-robot planning problems formulated by a generic factor graph defining dynamics and collision constraints. We show that our method allows extremely high performance collaborative planning in a simulated road traffic scenario, where vehicles are able to cross each other at a busy multi-lane junction while maintaining much higher average speeds than alternative distributed planning techniques. We encourage the reader to view the accompanying video demonstration to this work at <https://youtu.be/5d4LXbxgxaY>.

I. INTRODUCTION

As automation increases, multiple autonomous robotic devices will need to operate together in limited spaces, whether vehicles on a road network, or working robots in a home, farm or industrial setting. To achieve both safety and efficiency, these robots must unavoidably *coordinate* when planning their motions and other actions. At the most basic level, robots must take minimal account of each other's plans in order to avoid collisions. When coordination is stronger, extremely high efficiency is possible, with large numbers of devices moving smoothly around each other as they carry out their tasks.

It would often be assumed that highly coordinated planning requires centralised control, where a single computer receives state information from all robots and solves a unified multiple trajectory optimisation problem before sending commands back to them all. In this paper we show that remarkable performance is possible from an alternative distributed technique which uses efficient local per-robot computation and flexible purely peer-to-peer communication.

Our solution formulates multi-robot planning as a dynamic optimisation problem characterised by a factor graph with continuous variables representing robot poses and velocities over a bounded forward time window. These are connected by constraint terms which represent each robot's dynamics and the need to avoid collisions with other robots as well as static obstacles. Planning consists of performing inference on the factor graph to determine marginal distributions for the future poses which best satisfy all constraints.

To achieve distributed computation, the full joint factor graph is divided up into fragments which individual robots

have responsibility for storing and updating. The graph is optimised using Gaussian Belief Propagation (GBP), an iterative and distributed message passing algorithm which can achieve the same global solution as a centralised solver. Messages which need to be sent between the fragments held by different different robots can be efficiently transmitted by regular, efficient peer-to-peer communication. The particularly appealing property of GBP is that global convergence can be achieved with many types of communication schedule.

We demonstrate our algorithm in a simulation of robot vehicles moving through a busy traffic junction at high velocities, jointly planning to achieve extremely high continuous flow which is far beyond what has been demonstrated with alternative distributed planning techniques. We believe that our approach has broad applicability to any situation where robots need to cooperate in tight spaces.

II. RELATED WORK

Research on multi-robot path planning can be categorised into centralised and distributed algorithms. Centralised approaches make use of a central hub that has full knowledge of the states of all robots and constraints in the environment and return to each robot a planned trajectory to follow, but have obvious challenges with scaling and the requirement for all robots to have high bandwidth communication to hub. We therefore focus in this paper on distributed approaches which can operate with per-robot parallelism and require only peer-to-peer communication.

The problem of finding a globally optimal solution for the multi-robot trajectory planning problem in the presence of safety and dynamic constraints is NP-hard in general [1], and distributed approaches usually do not offer optimality guarantees. However, they can be extremely useful in practice, particularly for continuous accurate local replanning with dynamics rather than situations which require global search and maze-solving, where iterative solvers can work well. and produce trajectories that can cope with varying conditions and changes in the environment.

Distributed planners in their most essential form operate by performing conflict resolution when necessary to alter planned trajectories. In [2], priority-based algorithms effectively treat high priority robots as dynamic obstacles with unchanging trajectories and cause low priority robots to react in response.

When trajectories must be planned in real-time and finding a safe and efficient solution is more important than global optimality, iterative solvers can be used. Trajectories can

¹Aalok Patwardhan and Andrew J. Davison are with the Dyson Robotics Lab and the Department of Computing, Imperial College London [a.patwardhan21, a.davison]@imperial.ac.uk

²Riku Murai is with the Department of Computing, Imperial College London riku.murai15@imperial.ac.uk

be iterated until convergence, adapting to new obstacles or constraints that may be discovered. The work in [3] presents an online solver using Alternating Direction Method of Multipliers (ADMM) for a small number of robots moving through an environment with moving objects. The robots move together in formation and their paths do not intersect.

We believe that an important area of consideration is inter-robot communication to fully unlock the capabilities of distributed planning with regards to producing safe and efficient trajectories. Algorithms such as in [4] have shown that successful solutions can be obtained through inter-robot communication networks for robots approaching within sensing range of each other. The method in [5] makes use of inter-robot communication with robots restricted in communication range, and applies the novel use of graph neural networks (GNN) in a grid-world in distributed planning.

In our work we want to consider robots which have general kinematic and dynamic constraints, and are able to plan continuous trajectories. This is the domain of model-predictive control, and we are inspired in particular by methods like GPMP2 [6]. This is a method for a single robot in a known static environment, but importantly showed that planning with dynamics could be formulated as inference on a Gaussian factor graph, and therefore that general factor graph solvers such as GTSAM [7] which are normally used for estimation could be easily adapted to planning applications. The definition of all cost terms in a planning cost function as quadratic in a set of variables means that planning is solved by the same sparse least-squares inference computation as arises in robot estimation problems such as SLAM.

Very recently, Murai *et al.* showed in their Robot Web work [8] that a highly distributed solution to the distributed estimation problem of multi-robot localisation is possible using efficient distributed computation via Gaussian Belief Propagation. In this paper, we adapt very much the same methods now to the domain of multi-robot collaborative planning, and can take advantage of the same distributed computation structure. We will show that this enables breakthrough performance for highly coordinated coordinated multi-robot motion planning which is far beyond previous distributed planning techniques and is also highly flexible and general.

III. BACKGROUND

We formulate multi-robot planning as a dynamic graph with continuous variables representing the current and future states of any number of robots. Constraints on the robots' motion, which model their individual dynamics and their need to avoid collisions either with each other or with static obstacles, connect these variables. The constraints are independent of each other, and the product of all of them defines the cost function which must be minimised to determine optimal trajectories for all robots. This means that the graph is a factor graph, and we can tackle the planning problem by using familiar tools to perform factor graph inference. The main novelty in this paper is the first use

of Gaussian Belief Propagation to enable a fully distributed solution of general multi-robot planning.

A. Factor Graphs

Factor graphs are a general and flexible representation for the factorisation of a function. In particular, a joint probability distribution $p(V)$ is factorised with a factor graph as:

$$p(V) = \prod_j^{N_f} f_j(V_j), \quad (1)$$

where given a set of variables $V = \{\mathbf{v}_i\}_{i=1:N_v}$, a factor node f_j is connected to a subset of the variables, $V_j \subseteq V$. Graphically, factor graphs are bipartite, with undirected edges connecting variables and factors. Solvers such as GTSAM [7] exploit the sparsity revealed by the factor graph for efficient maximum a-posteriori (MAP) inference using sparse linear algebra, and such algorithms are efficient for centralised solvers which have full access to the graph.

B. Factor Graphs for Planning

Path planning can be viewed as a nonlinear least-squares problem, where the robot avoids collision while moving towards the goal. Whilst it is possible to solve the nonlinear least-squares problem directly, factor graph abstraction allows us to – both easily and intuitively – model and exploit the sparsity of the factorisation. Furthermore, under a Gaussian noise model assumption, performing MAP inference on a factor graph is equivalent to solving a nonlinear least-squares problem. This equivalence allows us to use a factor graph solver to optimise the nonlinear least-square path planning problem.

In multi-robot path planning, further complexities arise as no prior knowledge of the factor graph topology is available, and computation must be decentralised in order to be scalable. The graph changes its topology dynamically as the path is optimised, connecting and disconnecting the nodes at every optimisation step. Given these problems, there is a need for a highly flexible, decentralised solution.

C. Gaussian Belief Propagation

An alternative method to perform inference on a factor graph is Belief Propagation (BP). The clear advantage of BP methods, which operate using node-wise local computation and message passing, is that they allow distributed solutions where no single computer ever needs to store the whole graph. A subclass of BP, where all the factors and the variables are Gaussian distributions is called Gaussian Belief Propagation (GBP). Gaussian assumptions are overwhelmingly common and useful in robotics as they capture the distribution of real-world events.

In this application as in many others we will apply GBP to a general loopy. graph with cycles. In this case, loopy-BP does not have general convergence guarantees; however, when it converges, it converges to the exact marginal posterior means under the Gaussian assumption. Furthermore, GBP is generally stable and can solve challenging computer

vision tasks such as bundle adjustment [9], [10] and scene flow estimation [11]. In the context of a multi-robot system, RobotWeb uses GBP for decentralised and scalable localisation of over 1000 robots [8].

Performing marginal inference with GBP is simple. Variables send messages to factors, and factors send messages back, and the whole process iterates. Here, we will give an overview of how GBP works. See [8], [12], [13], [14] for a detailed derivation.

We represent the Gaussian distribution in information form as:

$$\mathcal{N}(\mathbf{x}; \boldsymbol{\mu}, \boldsymbol{\Sigma}) = \mathcal{N}(\mathbf{x}; \boldsymbol{\eta}, \boldsymbol{\Lambda}) , \quad (2)$$

where $\boldsymbol{\Lambda} = \boldsymbol{\Sigma}^{-1}$ and $\boldsymbol{\eta} = \boldsymbol{\Lambda}\boldsymbol{\mu}$. In GBP, variables V are assumed to be Gaussian; thus, each variable has a belief $b(\mathbf{v}_i) = \mathcal{N}^{-1}(\mathbf{v}_i; \boldsymbol{\eta}_i, \boldsymbol{\Lambda}_i)$. Factors $F = \{f_i\}_{i=1:N_f}$ are a probabilistic Gaussian constraint between variables. $f_i(V_j)$ is an arbitrary function that connects variables V_j , and it may be non-linear.

1) *Variable Belief Update:* A variable updates its belief by taking the product of all incoming messages from the factors:

$$b(\mathbf{v}_i) = \prod_{f \in n(\mathbf{v}_i)} \mathbf{m}_{f \rightarrow i}(\mathbf{v}_i) , \quad (3)$$

where $n(\mathbf{v}_i) \subseteq F$ is the set of factors that the variable \mathbf{v}_i is connected to, and $\mathbf{m}_{f \rightarrow i}(\mathbf{v}_i) = \mathcal{N}^{-1}(\mathbf{v}_i; \boldsymbol{\eta}_{f \rightarrow i}, \boldsymbol{\Lambda}_{f \rightarrow i})$ is the message from a factor to the variable. As we are using information form, product can be rewritten as a summation:

$$\boldsymbol{\eta}_i = \sum_{f \in n(\mathbf{v}_i)} \boldsymbol{\eta}_{f \rightarrow i} , \quad (4)$$

$$\boldsymbol{\Lambda}_i = \sum_{f \in n(\mathbf{v}_i)} \boldsymbol{\Lambda}_{f \rightarrow i} . \quad (5)$$

However, for conciseness, we will keep the use of product notation.

2) *Variable to Factor Message:* A message from variable to factor $f_j \in n(\mathbf{v}_i)$ is the product of all incoming factor to variable messages apart from the message from f_j :

$$\mathbf{m}_{\mathbf{v}_i \rightarrow j}(f_j) = \prod_{f \in n(\mathbf{v}_i) \setminus f_j} \mathbf{m}_{f \rightarrow i}(\mathbf{v}_i) . \quad (6)$$

3) *Factor Likelihood Update:* The likelihood of factor $f(V_j)$ with measurement function $\mathbf{h}(V_j)$, observation \mathbf{z}_s , and precision of the observation $\boldsymbol{\Lambda}_s$, can be expressed as a Gaussian distribution $\mathcal{N}^{-1}(V_j; \boldsymbol{\eta}_f, \boldsymbol{\Lambda}_f)$, where $\boldsymbol{\eta}_f = \boldsymbol{\Lambda}_s(\mathbf{z}_s - \mathbf{h}(V_j))$ and $\boldsymbol{\Lambda}_f = \boldsymbol{\Lambda}_s$. This however only holds if $\mathbf{h}(V_j)$ is linear. In the non-linear case, we linearise using first-order Taylor expansion: $\mathbf{h}(V_j) \approx \mathbf{h}(V_j^0) + \mathbf{J}(V_j - V_j^0)$. The likelihood of the linearised factor takes the form [12]:

$$\boldsymbol{\eta}_f = \mathbf{J}^\top \boldsymbol{\Lambda}_m (\mathbf{J}V_j^0 + \mathbf{z}_m - \mathbf{h}(V_j^0)) , \quad (7)$$

$$\boldsymbol{\Lambda}_f = \mathbf{J}^\top \boldsymbol{\Lambda}_m \mathbf{J} , \quad (8)$$

where V_j^0 is the linearisation point, the current state of the variables. In our work $\mathbf{z}_m = 0$ for all the factors, meaning that the factor energy is purely a function of the states.

4) *Factor to Variable Message:* A message from a factor to variable \mathbf{v}_i is:

$$\mathbf{m}_{f \rightarrow i}(\mathbf{v}_i) = \sum_{\mathbf{v}_j \in V_j \setminus \mathbf{v}_i} f(V_j) \prod_{\mathbf{v}_j \in V_j \setminus \mathbf{v}_i} \mathbf{m}_{\mathbf{v}_j \rightarrow f}(\mathbf{v}_j) . \quad (9)$$

We take the product between the factor likelihood and messages from $V_j \setminus \mathbf{v}_i$ before marginalising out all variables but \mathbf{v}_i .

IV. METHOD

We now explain the details of how we formulate multi-robot planning as a factor graph. Although GBP can optimise factor graphs for any type of Gaussian variables and factors, for the rest of the paper we will consider a 2D scenario where robots are modelled as objects with two degrees of movement freedom on a plane.

A robot moving through a 2D plane may be modelled with the linear, time-varying stochastic differential equation (LTV-SDE):

$$\dot{\mathbf{x}}_i = \mathbf{A}\mathbf{x}_i + \mathbf{B}\mathbf{u}_i + \mathbf{F}\mathbf{w}_i , \quad (10)$$

where

$$\mathbf{A} = \begin{bmatrix} \mathbf{0} & \mathbf{1} \\ \mathbf{0} & \mathbf{0} \end{bmatrix}, \mathbf{B} = \mathbf{0}, \mathbf{F} = \begin{bmatrix} \mathbf{0} \\ \mathbf{1} \end{bmatrix} , \quad (11)$$

and $\mathbf{w}_i \sim \mathcal{N}(\mathbf{0}, \mathbf{Q}_d)$ is white process noise with covariance matrix $\mathbf{Q}_d = \sigma_d^2 \mathbf{I}$.

As this work focuses on path planning, the known system control input \mathbf{u}_i is set to 0.

The state \mathbf{X}_i of a robot at time t_i represents the robot's position and velocity at that particular moment in time:

$$\mathbf{X}_i = [\mathbf{x}_i^\top, \dot{\mathbf{x}}_i^\top]^\top = [x_i, y_i, \dot{x}_i, \dot{y}_i]^\top . \quad (12)$$

The trajectory of a robot is represented by N such states, from the state \mathbf{X}_0 (the ‘‘robot head’’) at the current time t_0 to the state \mathbf{X}_{N-1} (the ‘‘robot goal’’) at time t_{N-1} .

The optimal trajectory solution can be found by solving for the maximum a posteriori (MAP) solution \mathbf{X}^* for the trajectory states. Since each state is only dependent on the state at the previous timestep, the states are all Markovian in time resulting in a sparse linear system.

A robot with look-ahead horizon t_{N-1} can plan its trajectory at discrete timesteps t_i into the future. In the presence of moving obstacles and other robots the safety of the robot is paramount. It is the states in the immediate future that are of more importance with respect to optimising a trajectory. The time gap $\Delta T_i = t_i - t_{i-1}$ between consecutive states X_{i-1} and X_i therefore increases further into the future of the planned trajectory. We consider the trajectory being comprised of several groups of M consecutive states. Within each group the time gap between states ΔT is constant. This time gap increases by 1 timestep per group of M states. An example trajectory of a rightward-moving robot with $M = 3$ can be seen in figure 1, showing the spacing between states.

Considering the planning problem as a factor graph allows for fast inference, with the nodes of the graph representing the robot states through time. Factors representing the trajectory smoothness and obstacle avoidance constraints are

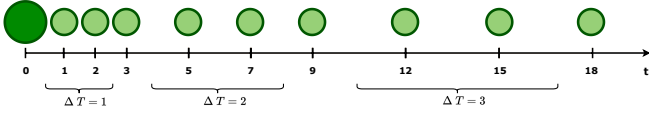


Fig. 1: Robot states are spaced out in time, shown here for $M = 3$. Each group of M states have a constant ΔT_i .

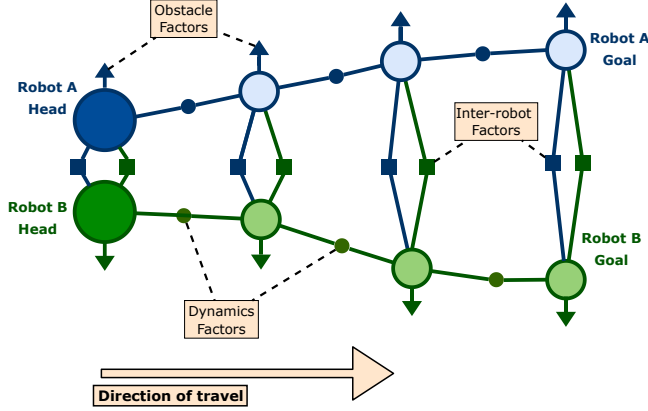


Fig. 2: An example factor graph with two robots (A and B) showing the various types of factors present. Note that unary pose factors f_p are connected to each robot's head and goal states but are not shown here.

connected to the nodes. There are four types of factors that we consider. A unary pose factor f_p is connected to the head and goal states and represents the prior information on the pose of the state. A dynamics factor f_d encourages a smooth trajectory and represents a noise-on-acceleration dynamics model. An obstacle factor f_o penalises a state from being close to a stationary obstacle in the scene. Finally an inter-robot factor f_r penalises trajectories that bring robots within collision range at a particular timestep, and takes into account each robot's future positions. An example of the resulting factor graph may be seen in figure 2.

A. Pose Factor

We define a unary pose factor f_p connected to the head and goal states of the robot with a measurement function:

$$\mathbf{h}_p(\mathbf{X}_i) = \mathbf{X}_i, \quad (13)$$

$$\Sigma_p = \sigma_p^2 \mathbf{I}. \quad (14)$$

The robot head and goal states (\mathbf{X}_0 and \mathbf{X}_{N-1}) are connected to strong pose factors with small values of σ_p , ensuring that the trajectory is anchored at these states during optimisation.

B. Dynamics Factor

For a trajectory to be smooth and dynamically feasible, each state of the robot is connected to the next in time via

a factor defined by:

$$\mathbf{h}_d(\mathbf{X}_i, \mathbf{X}_{i+1}) = \Phi(t_{i+1}, t_i) \mathbf{X}_i - \mathbf{X}_{i+1}, \quad (15)$$

$$\Sigma_d = \begin{bmatrix} \frac{1}{3} \Delta t_i^3 \mathbf{Q}_d & \frac{1}{2} \Delta t_i^2 \mathbf{Q}_d \\ \frac{1}{2} \Delta t_i^2 \mathbf{Q}_d & \Delta t_i \mathbf{Q}_d \end{bmatrix}, \quad (16)$$

where

$$\Phi(t_b, t_a) = \begin{bmatrix} \mathbf{1} & (t_b - t_a) \mathbf{1} \\ \mathbf{0} & \mathbf{1} \end{bmatrix}, \quad (17)$$

is the state transition matrix from time t_a to time t_b . This factor encourages a zero acceleration and therefore a feasible and smooth trajectory [6].

1) *Dynamic Factor Realignment (DFR)*: The GBP algorithm causes states to change in response to messages from their connected factors. Using the noise-on-acceleration dynamics model defined in IV, the process noise covariance matrix \mathbf{Q}_d is isotropic. This means that the states that the factor is connected to are equally likely to change in the x and y directions during trajectory optimisation.

Two robots approaching each other are able to modify their trajectories to avoid collision and swerve around each other, as expected for holonomic robots. This is seen in figure 4a.

To model realistic (non-holonomic) scenarios such as multi-agent path planning in an autonomous traffic case, agents would ideally avoid swerving by staying in their lanes and only accelerating or decelerating in the direction of their intended travel as seen in figure 4b. In this work the dynamic factors are realigned during trajectory optimisation so that their covariances are weaker in the direction of the robot's goal state, as seen in figure 3. For a dynamic factor connecting states \mathbf{X}_i and \mathbf{X}_{i+1} , dynamic factor realignment (DFR) happens every timestep and is done by first obtaining the unit vector $\hat{\lambda}$ from the position of state \mathbf{X}_i to that of the goal state \mathbf{X}_{N-1} . A transformation matrix \mathbf{T}_{DFR} is then constructed whose columns are $\hat{\lambda}$ and its orthogonal complement $\hat{\lambda}_\perp$. The factor covariance Σ_d is recalculated using the modified process noise covariance matrix:

$$\mathbf{Q}'_d = \mathbf{T}_{DFR} \mathbf{Q}_d \mathbf{T}_{DFR}^\top, \quad (18)$$

$$\mathbf{T}_{DFR} = [\hat{\lambda} \quad k_{DFR} \hat{\lambda}_\perp], \quad (19)$$

where $k_{DFR} = 0.1$ is a scaling parameter, and $\hat{\lambda}$ is the unit vector in the direction of the robot goal state.

C. Obstacle Factor

A unary factor is connected to each state of a robot, representing the distance of the state position from static obstacles in the environment. A 2D signed distance field (SDF) is calculated at the start of the simulation. The obstacle factor is defined by the measurement function $h_o(\mathbf{X}_i)$ which returns the value of the signed distance field at the state's position \mathbf{x} . This is equal to 1 at or within the obstacle boundary, decreasing exponentially to 0 at a distance of one robot radius away from the obstacle. The factor covariance matrix is $\Sigma_o = \sigma_o \mathbf{I}$. It is assumed that a robot can instantaneously query the value of the SDF at a point of interest in the environment.

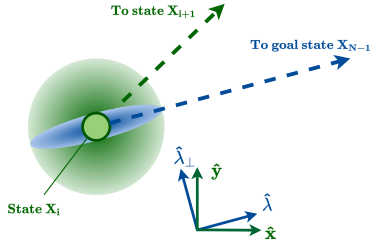


Fig. 3: Dynamic Factor Realignment: The green ellipse represents the isotropic covariance on the position of state X_i . The blue ellipse represents the covariance after DFR, now aligned towards the goal state. The green and blue dashed arrows show the directions from state X_i to state X_{i+1} and the goal state respectively.

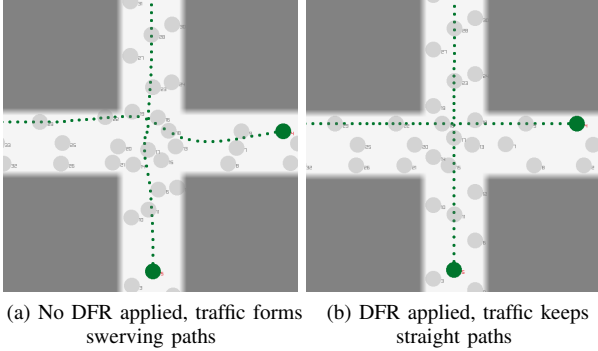


Fig. 4: Trajectories of two robots (green) through a busy traffic junction with (a) no DFR applied and (b) DFR applied.

D. Inter-robot Factor

If a robot A encounters another robot B within its sensor range, an inter-robot factor is created for each timestep of the robot trajectories. State $X_{A,i}$ of robot A is connected to state $X_{B,i}$ of robot B at all future timesteps $i \geq 1$. This ensures that robots will not occupy the same position at the same time (collide).

The factor has a non-zero energy cost if the distance between the robots at a particular timestep is less than the critical distance $r^* = 2r_{robot} + \epsilon$ where r_{robot} is the radius of a robot, and ϵ is a small ‘safety distance’. We first define a truncated hinge loss function $g(p)$ of the form:

$$g(p) = \begin{cases} 1 - \frac{p}{r^*} & p \leq r^* \\ 0 & \text{otherwise} \end{cases} \quad (20)$$

There is the possibility that robot trajectories could intersect in between two consecutive timesteps – this could happen if the spacing between states is sufficiently large due to a high robot velocity. To avoid this issue we allow for K-point linear interpolation between timesteps in the inter-robot factor. The factor is then defined with the measurement function:

$$h_r(X_{A,i}, X_{B,i}) = \left[g\left(r_{i+\frac{k}{K}}\right) \right]_{0 \leq k \leq K-1}, \quad (21)$$

where:

$$r_{i+\frac{k}{K}} = \left\| \mathbf{x}_{A,i} + \left(\frac{k}{K}\right) \dot{\mathbf{x}}_{A,i} - \mathbf{x}_{B,i} - \left(\frac{k}{K}\right) \dot{\mathbf{x}}_{B,i} \right\|, \quad (22)$$

is the distance between the two robots at the timestep $t_{i+\frac{k}{K}}$ calculated using the position and velocities at timestep t_i . The factor covariance matrix takes the form $\Sigma_r = \sigma_i \mathbf{I}$, where $\sigma_i = \sigma_r t_i$ such that the factor covariance is weaker for states further in the future.

It can be seen in Figure 2 that there are two inter-robot factors for each timestep of the trajectories. This symmetry in factor creation represents a shared responsibility between the two robots for planning safe trajectories but is also a redundancy in the design. In future work this could be extended further to allow heterogeneous robots to define their own trajectory parameters, such as safety thresholds or self-importance.

E. Goal State Update

At each timestep the goal position moves according to its target velocity \mathbf{v}^* as long as it is within some maximum distance r_{max} from the robot head. If this distance is exceeded, the goal state velocity is capped at the value of the component of the robot head’s velocity in the direction of \mathbf{v}^* .

Without this constraint, a slow or stationary robot (in the case of a traffic build-up or obstacle) would have a goal state that continued to move further away, leading to unrealistic accelerations due to the spacing between states increasing and the robot ‘jumping’ across the environment. The goal state X_{N-1} is updated as:

$$X_{N-1} \leftarrow \begin{bmatrix} \mathbf{x}_{N-1} + \tau \mathbf{v}_{N-1}^* \\ \mathbf{v}^* \end{bmatrix}, \quad (23)$$

where:

$$\tau = \begin{cases} 1 & \|\mathbf{x}_{N-1} - \mathbf{x}_0\| \leq r_{max} \\ (\dot{\mathbf{x}}_0 \cdot \mathbf{v}^*) & \text{otherwise} \end{cases} \quad (24)$$

and $r_{max} = t_{N-1} \|\mathbf{v}^*\|$.

F. Online Algorithm

Each robot performs Algorithm 1. At every timestep, when new robots are within sensor range of each other, inter-robot factors are created between them if they do not already exist, and destroyed when the robots are mutually out of range.

V. EVALUATION

Our method for multi-robot planning is highly general, but here we demonstrate it with a simulation based on a model of traffic on an advanced autonomous road network. We consider the intersection of two roads of length $D = 100m$ with $L = 3$ lanes in each, and simulate robots traversing this junction at different flowrates Q^* . This intersection is representative of junctions in a larger system, for example autonomous vehicles moving through a Manhattan-style grid of traffic, or robots moving through a factory floor. Each robot is modelled as a 2-dimensional circle of radius $2m$

Algorithm 1 For one robot R_i

- 1: Let $C(R_i)$ be a set of robots currently connected to R_i .
 - 2: Let $N(R_i) = \{R_j \mid \|R_i - R_j\| < r\}$ be a set of robots with in close proximity (r meters) to R_i .
 - 3: Perform n_1 GBP iterations to initialise trajectory
 - 4: **while** Running **do**
 - 5: **for** $R_j \in N(R_i) \setminus C(R_i)$ **do**
 - 6: Create inter-robot factors $f(R_i, R_j)$ with a newly observed robot.
 - 7: **end for**
 - 8: **for** $R_j \in C(R_i) \setminus N(R_i)$ **do**
 - 9: Delete inter-robot factors $f(R_i, R_j)$ with a robot out of range.
 - 10: **end for**
 - 11: Perform n_2 GBP iterations to adapt trajectory to newly created/destroyed factors
 - 12: Update the robot's belief (Sec. III-C.1).
 - 13: Perform Dynamic Factor Realignment (Sec. IV-B.1).
 - 14: Goal state update (Sec. IV-E).
 - 15: Perform n_1 GBP iterations to adapt trajectory to new states.
 - 16: **end while**
-

and mass $1000kg$ and has a target speed of $\|\mathbf{v}^*\| = 30ms^{-1}$, typical of a car travelling on a highway. The robot has a look-ahead horizon of $t_{N-1} = 30$ timesteps into the future, and a sensor range of $r_{sensor} = t_{N-1} \|\mathbf{v}^*\|$.

To achieve a desired flowrate of Q^* robots/s, new robots are added for each lane every $\frac{2L}{Q^*}(1+\epsilon)$ timesteps where $\epsilon \sim \mathcal{U}(0, 0.5)$ is a small uniformly distributed random parameter. In the event of a traffic jam, robots will not be able to reach their target velocities; a build-up will occur resulting in a lack of space to create new robots. As a result the actual flowrate Q (measured using the number of robots that pass a point at $\frac{D}{4}$ during the simulation) will be less than the desired flowrate Q^* .

A. Parameters

The duration of one timestep is $\frac{1}{30}s$, and each simulation is run for $t_{sim} = 250$ timesteps. With respect to the number of GBP iterations per timestep (as in Algorithm 1), $n_1 = 60$ and $n_2 = 5$ are values chosen empirically for the convergence of planned trajectories. The standard deviations of the pose, inter-robot and obstacle factors are $\sigma_p = 1 \times 10^{-15}$, $\sigma_r = 1 \times 10^{-5}$ and $\sigma_o = 1 \times 10^{-6}$ respectively. The standard deviation of the dynamics factor is set to $\sigma_d = \sqrt{10} \|\mathbf{v}^*\| \times 10^{-5}$. Since the dynamics factor effectively causes accelerations around a zero mean, we can consider an upper bound on the magnitude of robot accelerations to be $a_{max} = 3 \sigma_d m \text{ timestep}^{-2} = 0.467ms^{-2}$. This value is typical of the average accelerations of cars travelling at high speeds on a highway [15].

B. Metrics

We investigate the efficiency of our algorithm by varying the desired flowrate of robots through the intersection and

measuring two metrics of performance defined as

1) Mean of Average Speeds (MAS):

$$\frac{1}{N_R} \sum_R \frac{s_{r,final}}{t_{sim}}, \quad (25)$$

where $s_{r,final}$ is the displacement of robot r from its initial starting position to its final position at time t_{sim} . For smooth flow of traffic, this value should be as close as possible to the target speed of the robots $\|\mathbf{v}^*\|$.

2) Mean of Energy Consumption per metre (MEC):

$$\frac{1}{N_R} \sum_R \frac{e_r}{d_r}, \quad (26)$$

where d_r is the total distance travelled by robot r and e_r is the total energy consumed by robot r during positive acceleration. It is equivalent to the change in kinetic energy aggregated over each timestep.

If a robot has accelerated, it has increased its kinetic energy. For real world vehicles this would be equivalent to consuming more fuel and so robots moving in a smooth and efficient system would not have to accelerate much resulting in low energy consumption per metre, and average speeds close to their target speeds. Conversely, a high value for the MEC metric would be indicative of an inefficient system.

C. Constant Velocity Assumption (CVA) Baseline

We compare our collaborative GBP planner with a simple trajectory planning model where robots cannot communicate with each other but can only observe the position and velocities of the other robots around them. We imagine this to be similar to how human drivers, or simple decentralised path planning algorithms that prioritise safety would act. A robot extrapolates the positions of other robots in time using a constant velocity assumption based on their current velocities. We are able to adapt our existing GBP framework to this CVA model by using a new type of inter-robot factor defined here.

1) *Constant Velocity Assumption Factor*: If a robot A assumes that another robot B will keep moving at a constant observed velocity, it creates a factor f_{CVA} from each of its states to the head state of robot B. The factor is similar to the inter-robot factor f_r in section IV-D, except that it connects state $\mathbf{X}_{A,i}$ of robot A to the head state $\mathbf{X}_{B,0}$ of robot B. Similar to equation 21, the factor measurement function is $h_{CVA}(\mathbf{X}_{A,i}, \mathbf{X}_{B,0})$ with covariance matrix Σ_{CVA} .

Robot A extrapolates robot B's current position into the future to ensure a collision-free path. To ensure that the factor only affects the states of robot A, we set the entries corresponding to robot B's head state in the factor Jacobian to $\mathbf{J}(\mathbf{X}_{A,i}, \mathbf{X}_{B,0}) = \frac{\partial h}{\partial \mathbf{X}_{B,0}} = \mathbf{0}$.

VI. RESULTS AND DISCUSSION

Simulations were run for 250 timesteps for both the collaborative GBP and Constant Velocity Assumption models, varying the desired flowrate Q^* from 3 robots/s to 45 robots/s although it is the measured flowrates and densities that we plot the metrics against in figures 5 to 8. As discussed

Q^* (robots/s)	6	12	27	39
GBP Planner				
Q (robots/s)	4.7	9.7	40.3	41.4
CVA Planner				N/A
Q (robots/s)	4.8	12.7	19.0	

TABLE I: Qualitative comparison of planning performance for our GBP Planner and the Constant Velocity Assumption (CVA) planner at increasing desired traffic flow rates Q^* through the junction. The dots on selected robot trajectories are plotted at constant time intervals, and their pattern reveals the smoothness of traffic flow. We see that the CVA planner causes substantial stop and start behaviour in traffic beyond a flow of 12 robots per second where GBP still achieves extremely smooth motion. GBP still allows traffic to move well even up to extremely high desired flow rates as shown at 27 and 39 robots/s, where CVA completely breaks down in gridlock. Please see our accompanying video for an animated demonstration: <https://youtu.be/5d4LXbxgxaY>.

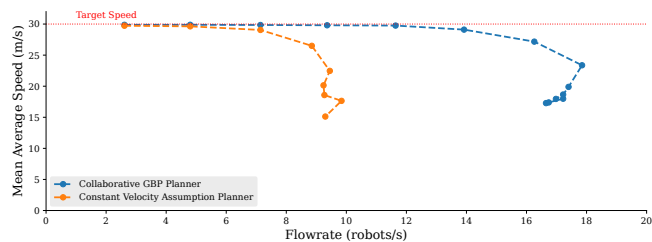


Fig. 5: Mean of Average Speeds (MAS) plotted against the *measured* flowrate Q , for each desired flowrate Q^* from 3 to 45 robots/s. Our GBP planner achieves a higher peak flowrate compared to the CVA planner and achieves target speed even at a high flowrate.

in Section V, the actual flowrate Q was often less than the desired flowrate due to traffic build-ups preventing new robots being created. Metrics were collected and averaged over 5 such simulation runs.

At low flowrates both models can produce Mean of Average Speeds (MAS) metrics at near target speeds, with the MAS generally decreasing as the flowrate increases (and with decreasing inter-robot spacing). The collaborative GBP planner performs near target speeds at much higher flowrates than the CVA planner as seen in Figure 5.

Figure 5 shows that MAS begins to deviate from the target speed at around 7 robots/s for the CVA planner. This is because as traffic build-up begins to occur and as a result, the CVA planner simulation is not carried out for measured flowrates higher than 10 robots/s. The MAS in the GBP

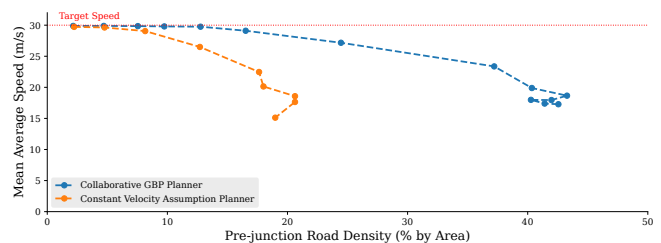


Fig. 6: MAS plotted against the Road Density, for each desired flowrate Q^* from 3 to 45 robots/s. Our GBP planner achieves higher density compared to the CVA planner, whilst maintaining a safe inter-robot distances.

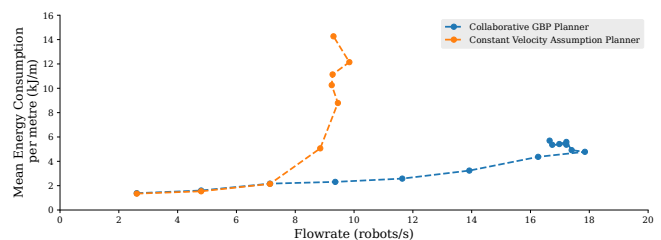


Fig. 7: Mean Energy Consumption per metre plotted against the *measured* flowrate Q , for each desired flowrate Q^* from 3 to 45 robots/s. Our GBP planner achieves lower energy consumption per metre with higher flowrates as compared to the CVA planner, highlighting that our solution leads to efficient traffic.

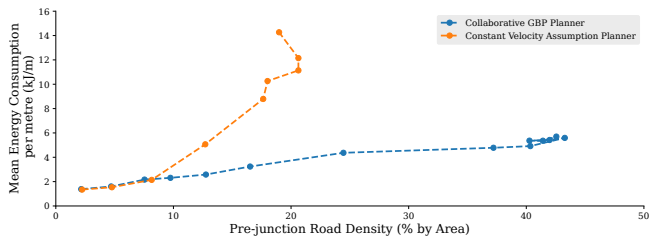


Fig. 8: Mean Energy Consumption per metre plotted against road density, for each desired flowrate Q^* from 3 to 45 robots/s. Our GBP planner achieves lower energy consumption per metre with higher densities as compared to the CVA planner. Our approach allows efficient traffic flow while being densely packed.

model begins to drop at a higher measured flowrate of 14 robots/s. Figure 5 shows the GBP curve folding back on itself at very high flowrates. This is because as maximum road capacity is approached, slower moving densely packed robots move at the same flowrate as faster moving robots with larger inter-robot gaps.

Figure 6 plots the MAS for the same experiments against road density ρ : the area taken up by robots as a percentage of the road. We consider the vertical and horizontal stretches of road before the intersection, and calculate the proportion of that area where robots are present. The road density will not reach $\rho = 100\%$ as we model the robots as circles with safety margins, and the width of a lane is greater than 1 robot diameter.

For the same simulations, Figures 7 and 8 show the MEC metric plotted against measured flowrate Q and road density ρ respectively for both GBP and CVA models. As Q and ρ increase, the MEC also increases. At low flowrates both the CVA and GBP planners perform similarly, as seen in table I. This is a result of the large inter-robot gaps which allow for non-intersecting trajectories. As the flowrate increases a sharp increase in MEC is observed for the CVA model whereas the metric for the GBP model continues to increase at a lower rate, allowing for higher efficiency traffic at a minor cost.

On highways it is recommended that vehicles leave a gap of $2s$ between themselves and the vehicle in front. At the target speed of $30ms^{-1}$ considered in this work ($100kmh^{-1}$) this would mean an inter-robot gap of $60m$, or a flowrate of 0.1 robots/s considering all 6 lanes of traffic. Our collaborative GBP framework allows vastly higher flowrates and therefore much smaller inter-robot distances whilst still guaranteeing collision-free trajectories. Robots are able to seamlessly navigate through intersecting lanes of traffic at or near their target speeds while maintaining safe and efficient trajectories.

VII. CONCLUSIONS

We have shown that the collaborative GBP planner can ensure smooth flow of traffic for high flowrates simply through message passing between robots in a purely peer-

to-peer manner. Highly efficient and safe trajectories are able to be planned for vehicles crossing at a busy junction, eliminating the need for a centralised control system and allowing the problem to be scaled up to many robots. Our current experiments are based on multiple iterations of communication between robots per motion step, but the results in [8] on multi-robot localisation using GBP offer a lot of promise that good factor graph optimisation and therefore planning performance could be achieved with much more efficient inter-robot communication patterns.

In the future, we will explore other applications of GBP planning, such as coordination of large numbers of robots which can organise themselves into useful formations.

ACKNOWLEDGEMENTS

Research presented in this paper has been supported by Dyson Technology Ltd. We are also grateful to many researchers with whom we have discussed some of the ideas in this paper, especially from the Dyson Robotics Lab and Robot Vision Group at Imperial College London. We would particularly like to thank Joe Ortiz and Tristan Laidlow.

REFERENCES

- [1] Jingjin Yu. Intractability of optimal multi-robot path planning on planar graphs. *CoRR*, abs/1504.02072, 2015.
- [2] J.P. van den Berg and M.H. Overmars. Prioritized motion planning for multiple robots. In *2005 IEEE/RSJ International Conference on Intelligent Robots and Systems*, pages 430–435, 2005.
- [3] Ruben Van Parys and Goele Pipeleers. Online distributed motion planning for multi-vehicle systems. In *2016 European Control Conference (ECC)*, pages 1580–1585, 2016.
- [4] C.M. Clark, S.M. Rock, and J.-C. Latombe. Motion planning for multiple mobile robots using dynamic networks. In *2003 IEEE International Conference on Robotics and Automation (Cat. No.03CH37422)*, volume 3, pages 4222–4227 vol.3, 2003.
- [5] Qingbiao Li, Fernando Gama, Alejandro Ribeiro, and Amanda Prorok. Graph neural networks for decentralized multi-robot path planning. In *2020 IEEE/RSJ International Conference on Intelligent Robots and Systems (IROS)*, pages 11785–11792, 2020.
- [6] Mustafa Mukadam, Jing Dong, Xinyan Yan, Frank Dellaert, and Byron Boots. Continuous-time gaussian process motion planning via probabilistic inference. *CoRR*, abs/1707.07383, 2017.
- [7] F. Dellaert. Factor graphs and GTSAM. Technical Report GT-RIM-CP&R-2012-002, Georgia Institute of Technology, 2012.
- [8] Riku Murai, Joseph Ortiz, Sajad Saeedi, Paul HJ Kelly, and Andrew J Davison. A robot web for distributed many-device localisation. *arXiv preprint arXiv:2202.03314*, 2022.
- [9] Joseph Ortiz, Mark Pupilli, Stefan Leutenegger, and Andrew J Davison. Bundle adjustment on a graph processor. In *Proceedings of the IEEE/CVF Conference on Computer Vision and Pattern Recognition*, pages 2416–2425, 2020.
- [10] Joseph Ortiz, Talfan Evans, Edgar Sucar, and Andrew J Davison. Incremental abstraction in distributed probabilistic slam graphs. *Proceedings of the IEEE International Conference on Robotics and Automation (ICRA)*, 2021.
- [11] Raluca Scona, Hidenobu Matsuki, and Andrew J Davison. From scene flow to visual odometry through local and global regularisation in markov random fields. *IEEE Robotics and Automation Letters*, 2022.
- [12] Andrew J Davison and Joseph Ortiz. Futuremapping 2: Gaussian belief propagation for spatial ai. *arXiv preprint arXiv:1910.14139*, 2019.
- [13] Joseph Ortiz, Talfan Evans, and Andrew J Davison. A visual introduction to gaussian belief propagation. *arXiv preprint arXiv:2107.02308*, 2021.
- [14] Christopher M Bishop and Nasser M Nasrabadi. *Pattern recognition and machine learning*, volume 4. Springer, 2006.
- [15] P.S. Bokare and A.K. Maurya. Acceleration-deceleration behaviour of various vehicle types. *Transportation Research Procedia*, 25:4733–4749, 2017. World Conference on Transport Research - WCTR 2016 Shanghai. 10-15 July 2016.